Tetrahedra system $Cu_4OCl_6daca_4$: High-temperature manifold of molecular configurations governing low-temperature properties

O. Zaharko,[1,*] J. Mesot,[1] L. A. Salguero,[2] R. Valentí,[2] M. Zbiri,[3] M. Johnson,[3] Y. Filinchuk,[4] B. Klemke,[5] K. Kiefer,[5] M. Mys'kiv,[6] Th. Strässle,[1] and H. Mutka[3]

[1]*Laboratory for Neutron Scattering, ETHZ & PSI, CH-5232 Villigen, Switzerland*

[2]*Institut für Theoretische Physik, Universität Frankfurt, D-60438 Frankfurt, Germany*

[3]*Institut Laue-Langevin, 156X, F-38042 Grenoble Cedex 9, France*

[4]*Swiss-Norvegian Beamlines, ESRF, F-38042 Grenoble Cedex 9, France*

[5]*BENSC, Hahn-Meitner Institut, D-14109 Berlin, Germany*

[6]*Institute for Inorganic Chemistry, Ivan Franko National University, 79005 Lviv, Ukraine*

(Received 8 January 2008; revised manuscript received 5 May 2008; published 4 June 2008)

The $Cu_4OCl_6daca_4$ system composed of isolated Cu^{2+} $S=1/2$ tetrahedra with antiferromagnetic exchange should exhibit the properties of a frustrated quantum spin system. *Ab initio* density functional theory calculations for electronic structure and molecular dynamics computations suggest a complex interplay between magnetic exchange, electron delocalization, and molecular vibrations. Yet, extensive experimental characterization of $Cu_4OCl_6daca_4$ by means of synchrotron x-ray diffraction, magnetization, specific heat, and inelastic neutron scattering reveal that properties of the real material can be only partly explained by proposed theoretical models as the low-temperature properties seem to be governed by a manifold of molecular configurations coexisting at high temperatures.

DOI: 10.1103/PhysRevB.77.224408 PACS number(s): 75.50.Xx, 36.40.Cg, 63.22.−m

I. INTRODUCTION

Strongly frustrated quantum spin systems show, following numerous theoretical works,[1–5] highly degenerate ground states. When the degeneracy is lifted, a number of exotic ground states may emerge. However, in spite of large experimental efforts, such examples are rare and are hard to probe. Any perturbation tends to push the real system into a conventional classical ground state. A good recent example is the $Cu_2Te_2O_5X_2$ (X=Cl,Br) system. Assumed to be built of weakly coupled tetrahedral units,[6–11] it appears to have an incommensurate three-dimensional long-range ordered ground state.[12]

Our aim is to investigate the properties of tetrahedra which are the building blocks of geometrically frustrated quantum spin lattices (e.g., kagomé and pyrochlore). Note that the ground state of an isolated tetrahedron with antiferromagnetic Heisenberg exchange is doubly degenerate in the case of high T_d symmetry. It is formed by two entangled[11,14] singlets: one is a product of two dimers $\psi_1=\frac{1}{\sqrt{4}}(|\uparrow\uparrow\downarrow\downarrow\rangle+|\downarrow\downarrow\uparrow\uparrow\rangle-|\uparrow\downarrow\downarrow\uparrow\rangle-|\downarrow\uparrow\uparrow\downarrow\rangle)$ and the second is composed by two-site triplet products, $\psi_2=\frac{1}{\sqrt{12}}(2|\uparrow\downarrow\uparrow\downarrow\rangle+2|\downarrow\uparrow\downarrow\uparrow\rangle-|\uparrow\uparrow\downarrow\downarrow\rangle-|\uparrow\downarrow\downarrow\uparrow\rangle-|\downarrow\downarrow\uparrow\uparrow\rangle-|\downarrow\uparrow\uparrow\downarrow\rangle)$. Three triplets and one quintet constitute the excited states. We choose in the present work a simple frustrated quantum spin candidate among zero-dimensional systems.

We focus our study on the $Cu_4OCl_6L_4$ system. Its main magnetic building block is an almost ideal isolated tetrahedral cluster of four Cu^{2+} ions (see Fig. 1). The magnetic properties of several representatives of this family could not be quantitatively accounted for by a simple Heisenberg isotropic exchange.[15–17] A number of more complex models have been proposed. In early stages, Lines *et al.*[15] suggested the existence of orbital degeneracy of the Cu^{2+} ion and a large antisymmetric contribution to the spin Hamiltonian. However, angular overlap model calculations[18] indicate that the unpaired electron of the Cu^{2+} ion occupies the dz^2 nondegenerate orbital with no orbital moment, which is around 960 meV above other d orbitals.

Henceforth, the invoked models follow two routes; the first one exploits the complexity of the spin exchange and the second one puts forward the spin-vibrational interactions. The first approach is based on the generalized spin Hamiltonian

$$H_{ex}=H_{iso}+H_{as}+H_{an}=\sum_{i,j}J_{ij}\mathbf{S}_i\mathbf{S}_j+\sum_{i,j}\mathbf{G}_{ij}(\mathbf{S}_i\times\mathbf{S}_j)+\sum_{i,j}\sum_{\alpha=x,y,z}J_{ij}^{\alpha}\mathbf{S}_i^{\alpha}\mathbf{S}_j^{\alpha}, \quad (1)$$

where H_{iso} is the isotropic Heisenberg–Dirac–Van Vleck

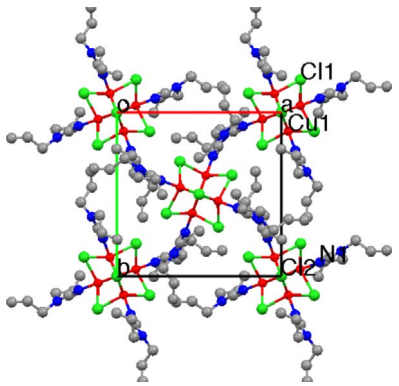

FIG. 1. (Color online) The *ab* projection of the $Cu_4OCl_6daca_4$ unit cell. Cu atoms are represented by red circles and Cl, N, and C atoms by green, blue, and gray circles, respectively. H atoms are omitted for clarity; O atoms are located behind Cl2 and, therefore, are not visible.

TABLE I. Comparison of the characteristic angles (deg) and intra- (d_{intra}) and inter- (d_{inter}) molecule distances (Å) in $Cu_4OCl_6daca_4$ at 80 and 300 K. Mean-square displacement amplitudes of Cu (MSD_{Cu}, in $Å^2$) and other atoms (MSD_{lig}, in $Å^2$) in the specified bond directions of the $CuCl_3ON$ trigonal bipyramid calculated from the anisotropic displacement parameters refined at 80 K.

d_{intra}	80 K	300 K	Angle	80 K	300 K
Cu-Cu	3.0790(2)	3.0933(4)	$\angle_{CuOCu}$	108.106(6)	108.9(2)
Cu-Cu	3.1183(2)	3.1101(5)	$\angle_{CuOCu}$	110.158(6)	109.8(2)
Cu-O	1.9016(2)	1.9011(3)	$\angle_{NCuO}$	179.01(4)	178.8(1)
Cu-N1	1.932(1)	1.935(3)	$\angle_{CuCl1Cu}$	80.46(1)	80.48(3)
Cu-Cl1	2.3694(4)	2.3911(9)	$\angle_{CuCl2Cu}$	80.59(1)	80.62(3)
Cu-Cl2	2.3806(3)	2.3909(8)	$\angle_{Cl1CuCl1}$	117.97(2)	118.85(4)
Cu-Cl1	2.4578(3)	2.4231(9)	$\angle_{Cl1CuCl2}$	127.73(1)	120.92(3)
	MSD_{Cu}	MSD_{lig}	d_{inter}	80 K	300 K
Cu-O	0.0107	0.0125	d_{100}	12.60490(3)	12.5652(1)
Cu-Cl1	0.0143	0.0130	d_{001}	12.73045(5)	13.7685(2)
Cu-Cl2	0.0203	0.0189	d_{111}	10.9525(3)	11.2399(1)
Cu-N1	0.0108	0.0152			

term and H_{as} and H_{an} are the antisymmetric and anisotropic terms, respectively. A number of authors[17,19,20] explained magnetic susceptibility, electron paramagnetic resonance, and inelastic neutron scattering (INS) observations by considering large antisymmetric contributions (up to 20% of the isotropic exchange constant). Dickinson *et al.*[21] suggested the presence of ferromagnetic intercluster exchange in addition to the antiferromagnetic intracluster one.

The second approach is based on the spin-vibrational Hamiltonian

$$H = H_{vib}(q) + H_{ex}(S,q), \tag{2}$$

where $H_{vib}(q)$ describes the harmonic vibration of the nuclei around the equilibrium position and $H_{ex}(S,q)$ depends not only on the spin S but also on the nuclear displacements q of the Cu^{2+} ions. Jones[16] developed a simplified model of dynamic and fluxional Jahn–Teller distortions of $Cu_4OCl_6L_4$, assuming a linear relation between the coupling constants and the atomic shifts. Polinger *et al.*[22,23] extended this approach concluding that the pseudo-Jahn–Teller effect is the most probable reason for the anomalous magnetic properties of the system.

We collected substantial experimental data on $Cu_4OCl_6L_4$ with L=diallylcyanamide=N≡C-N-$(CH_2$-CH=$CH_2)_2$ ($Cu_4OCl_6daca_4$) and performed *ab initio* density functional theory calculations for the electronic structure as well as *ab initio* molecular dynamics computations. Our findings suggest that, indeed, the vibrational degrees of freedom are very important. However, the dominant ingredient is the presence of a manifold of molecular configurations coexisting at high temperatures. Therefore, both the generalized spin and the spin-vibrational Hamiltonians remain insufficient to explain the measured magnetic properties of $Cu_4OCl_6L_4$.

II. EXPERIMENTAL DETAILS

$Cu_4OCl_6daca_4$ single crystals (Nr. 1 and Nr. 2) and a polycrystalline sample have been prepared by a reaction between CuCl and diallylcyanamide in the presence of I_2.[24] The crystal structure has been examined by x-ray synchrotron powder and single crystal diffraction performed at the BM01A Swiss-Norvegian Beamline of the European Synchrotron Radiation Facility (ESRF; Grenoble, France) at a wavelength of 0.7272 Å in the 16–340 K temperature range.

The bulk properties have been studied using a commercial Quantum Design physical property measurement system. The dc- and ac-magnetic susceptibilities of polycrystalline and single crystal materials have been measured in the 1.8–300 K temperature range and in applied magnetic fields of up to 9 T. The measurements have been performed mostly on cooling with a cooling speed of 0.5 K/min. Specific heat data have been obtained in the 0.35–10 K temperature range and in applied magnetic fields of up to 14.5 T and magnetization data in the 1.8–20 K temperature range for up to 14.5 T.

Inelastic neutron scattering experiments have been performed on a 2 g polycrystalline protonated $Cu_4OCl_6daca_4$ sample on the neutron time-of-flight spectrometer FOCUS at the spallation neutron source SINQ (Paul Scherrer Institute, Switzerland) and on a 0.5 g polycrystalline deuterated sample on IN4 at the Institut Laue-Langevin (ILL; Grenoble, France). Four setups of FOCUS have been exploited (λ_i =5.45, 4.87, 3.42, and 2.26 Å) to access the 0–13 meV energy-transfer range with various energy resolutions. On IN4, high-energy transfers up to 40 meV have been probed with λ_i=1.32 Å, while a setup with λ_i=2.64 Å has been used for comparison with the FOCUS results on the protonated sample. All empty sample holders have been measured and subtracted.

III. CALCULATION METHOD

A. Electronic structure

In order to understand the electronic and magnetic properties in this compound, first principles local spin density approximation calculations were done within the framework

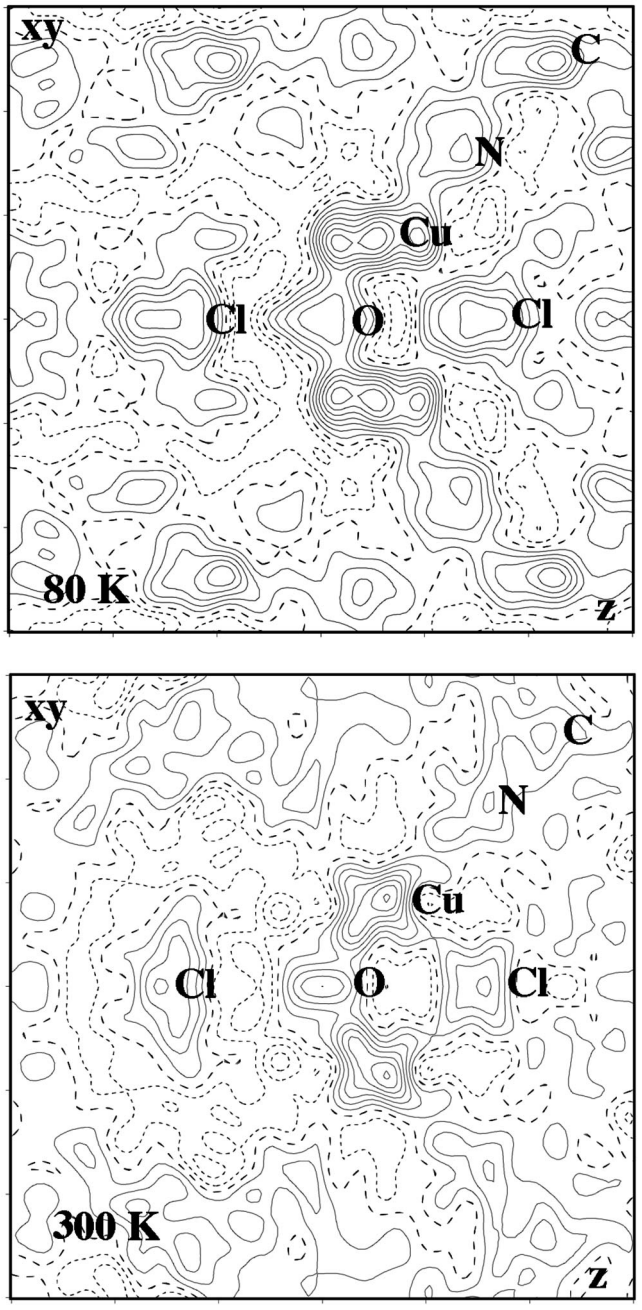

FIG. 2. Difference Fourier map of $Cu_4OCl_6daca_4$ at 80 K (top) and 300 K (bottom) from x-ray single crystal data.

of the density functional theory (DFT). For the description of the exchange and correlation energy, the generalized gradient approximation (GGA) was formulated by the Perdew–Burke–Ernzerhof (PBE) density functional.[25]

In the spin-polarized version of the GGA, the exchange-correlation energy E_{xc} is a functional of the local electron spin densities $n_\uparrow$ and $n_\downarrow$ and their gradients

$$E_{xc}^{GGA}[n_\uparrow,n_\downarrow] = \int f(n_\uparrow,n_\downarrow,\nabla n_\uparrow,\nabla n_\downarrow). \quad (3)$$

For calculating the eigenvalues and eigenvectors in the DFT scheme, the full potential linearized augmented plane

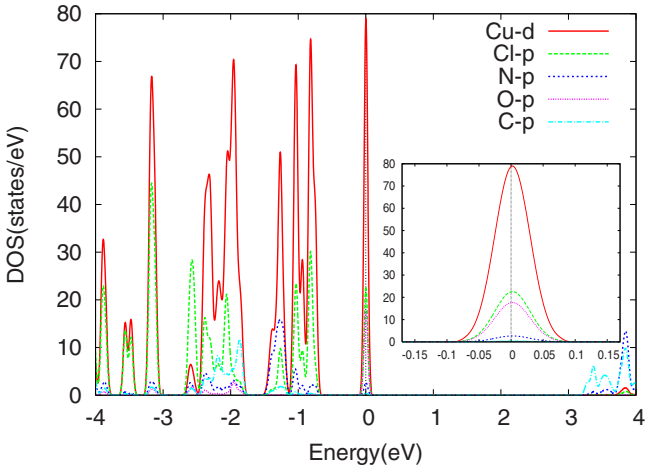

FIG. 3. (Color online) Partial density of states in the non-spin-polarized GGA calculations for $Cu_4OCl_6daca_4$ at $T=80$ K.

wave (LAPW) method, as implemented in the WIEN2K code,[26] has been used. In this method, the unit cell is divided in two regions; the first one is composed by nonoverlapping spheres centered at the atomic sites, and the second is the region between the atomic spheres or the interstitial region. In the first region, a spherical potential is assumed and, therefore, the wave functions are expanded in terms of spherical harmonics. In the interstitial region, a constant potential is assumed. This allows us to expand the wave functions in that region in terms of plane waves.

In our calculation, the valence wave functions have been expanded up to $l=10$. Sphere radii R_{mt} of 2.1 a.u. for the Cu atom and 1.6, 1.4, 1.2, 0.9, and 0.84 a.u. for Cl, O, N, C, and H atoms, respectively, have been set. Within the Cu muffin-tin radii chosen, we excluded the 4*s* states (the average radii for the wave functions belonging to these states is 2.7 a.u.); therefore, these states lie in the interstitial region. The Cu 3*d* and 3*p* states enter in the calculation as the valence and semicore states. respectively. For the Cu 3*d* states, the LAPW basis with augmented plane wave plus local orbital method have been used. The plane-wave expansion with $R_{MT}K_{MAX}$ equal to 3.76 has been set. This is a typical value when C–H bonds are present. For the integration in the irreducible wedge, 48 *k* points have been used.

B. Molecular dynamics

The dynamics of Cu-daca has been investigated using the DFT code VASP,[27,28] which is well adapted to a system as large as $Cu_4OCl_6daca_4$ (174 atoms per unit cell). VASP uses a plane-wave basis set and the projector augmented wave pseudopotentials to describe the core electrons of the atoms. The GGA-PBE functional was used[25] and all electronic calculations were performed at the Γ point in reciprocal space. Since phonons and molecular vibrations are of interest in this paper, lattice dynamics calculations, involving the determination of the dynamical matrix, were attempted. In view of the number of atoms in the unit cell, the direct method[29] is the only practically feasible approach in which symmetry-inequivalent atoms are displaced one by one from equilib-

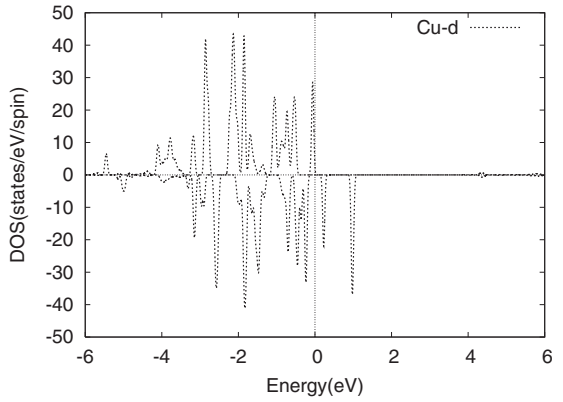

FIG. 4. Partial density of states for majority (upper panel) and minority (lower panel) spin contributions from Cu *d* states of $Cu_4OCl_6daca_4$ at $T=80$ K.

rium and the Hessian is constructed from the Hellmann–Feynman forces from the series of electronic calculations.

In the case of $Cu_4OCl_6daca_4$, the direct method always results in negative frequencies. This method invokes a significant perturbation to the equilibrium configuration and, therefore, the electronic structure. Indeed, electronic and structural correlations between the core and the ligands lead to an electronic structure which is very sensitive to the precise molecular configuration. Such sensitivity is an indication of the fragility of this molecular system, as proved by the physical meaning of negative frequencies in this case.

In this situation, we resorted to *ab initio* molecular dynamics, using VASP, in which case the (partial) vibrational density of states [(p)vDOS] can be obtained from the velocity autocorrelation function and the scattering function is obtained from the Van Hove correlation functions. Both of these correlation functions are determined directly from the *ab initio* molecular dynamics (AIMD) trajectories using the nMOLDYN program.[30] The temperature dependence of the dynamics, which may reveal anharmonicities, is investigated via the average kinetic energy of the atoms. The drawback of the molecular dynamics approach compared to a lattice dynamics calculation is that the phase relation of the atomic displacements is lost and normal modes and their frequencies cannot be determined. One solution is to investigate the time-dependent fluctuations of geometric quantities associated with groups of atoms. In the case of the magnetic properties of $Cu_4OCl_6daca_4$, the Cu tetrahedron is of interest.

AIMD simulations have therefore been performed at 100 and 250 K for a protonated crystal. Production simulations at constant volume and energy (*NVE* ensemble) cover 10 ps, that is, $\approx 10^4$ simulation steps. The 100 K simulation was then re-equilibrated for a deuterated crystal and the *NVE* production run in this case lasted 27 ps in order to give better access to the low frequency modes.

IV. RESULTS

A. Crystal structure

The $Cu_4OCl_6daca_4$ structure is tetragonal[24] (space group $P\bar{4}2_1c$) in the whole 16–340 K studied temperature interval.

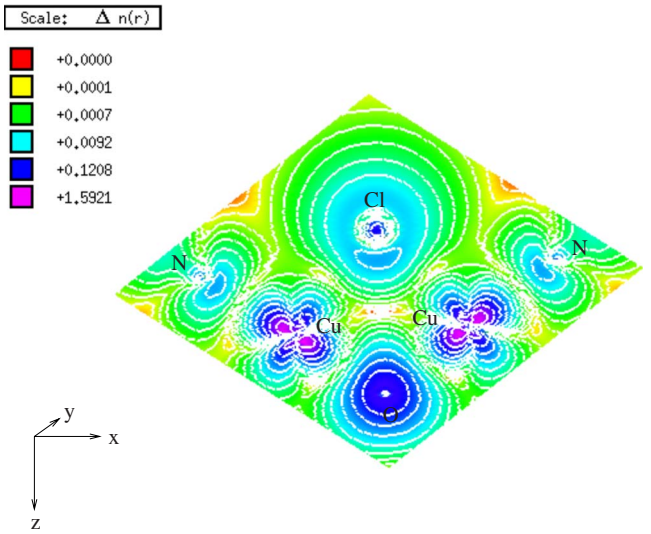

FIG. 5. (Color online) Charge density distribution at $T=80$ K.

There are two $Cu_4OCl_6daca_4$ molecules per unit cell, and they are slightly twisted around the *z* axis (Fig. 1). The oxygen is in the center of the molecule, surrounded by a tetrahedron of Cu^{2+} ions with two different Cu-Cu distances, equal to 3.0790(2) and 3.1185(2) Å at 80 K. The tetrahedron is enclosed by a distorted octahedron of chlorine ions with four Cl_1 in the square base and two Cl_2 in the apexes. Each copper has trigonal bipyramidal coordination: three Cl^- ions form the triangular base of the bipyramid, while the central O^{2-} ion and a terminal ligand *L* are located in apical positions. The exchange paths Cu-O-Cu are identical, while the two paths through chlorine ions, Cu-Cl_1-Cu and Cu-Cl_2-Cu, slightly differ (see Table I). Such geometry implies rather high symmetry of the cluster and of the spin exchange Hamiltonian, only marginally deviating from T_d.

There is an anomaly in the lattice constants in the 230–280 K temperature range notifying an isostructural order-disorder crossover.[31] Apparently, the molecule attains several configurations with a small energy difference between them. Above $T_C=282$ K these configurations coexist, while below T_C molecules freeze-in one of them. The configurations differ mainly by the position of the branched diallylcyanamide ligands, which fold. This modifies the distances between the molecules (Table I) and the unit cell volume shrinks by 7% at 80 K compared to the volume at room temperature. The $Cu_4OCl_6N_4$ core changes very little. The only noticeable difference is the shift of the Cl_1 ions by 0.2487(9) Å, while for Cu and Cl_2 the shift is only 0.0462(9) and 0.0282(9) Å, respectively.

Inspection of the interatomic distances and angles presented in Table I suggests that the Cu-O-Cu magnetic exchange path is antiferromagnetic (AF), while the Cu-Cl-Cu one is ferromagnetic (F). Therefore, the mobility of the Cl_1 ions is essential in determining the magnetic exchange and this is investigated with the help of AIMD simulations.

One more appreciable detail could be extracted from the single crystal diffraction data. The difference Fourier map through the N-O-N plane of the molecule (Fig. 2) shows

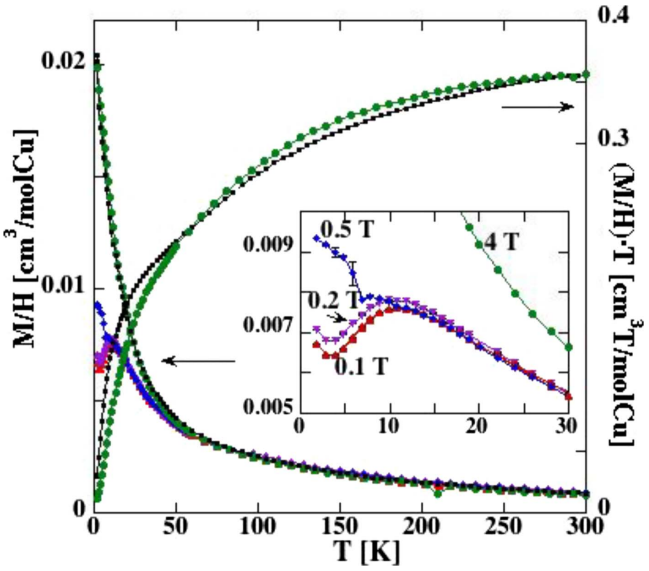

FIG. 6. (Color online) Temperature dependence of the dc magnetizations (M/H) of the single crystal Nr. 1 measured at 0.1, 0.2, 0.5, and 4 T and of polycrystalline (black solid line) $Cu_4OCl_6daca_4$ measured at 0.1 T (left scale). $(M/H)T$ of the crystal and the powder measured at 0.1 T (right scale). Inset: Zoomed 1.8–30 K temperature interval of M/H of the crystal.

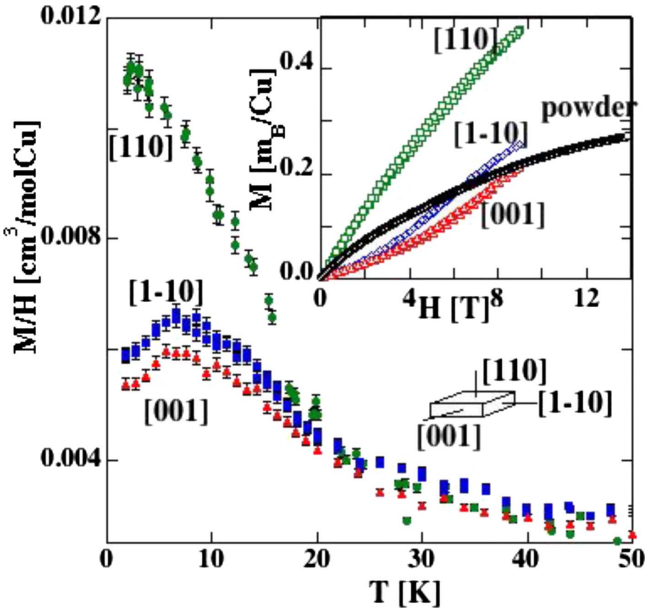

FIG. 7. (Color online) Temperature dependence of dc magnetization (M/H) of the single crystal Nr. 2 measured with magnetic field $H=0.2$ T applied along three crystallographic directions: [110] (green circles), [001] (red triangles) and $[\bar{1}10]$ (blue squares), corresponding to short, middle, and long edges of the crystal. Inset: Field dependence of dc magnetization of single crystal Nr. 2 and powder $Cu_4OCl_6daca_4$ at 1.8 K.

additional electron density near Cu atoms at 80 K. The tiny peaks (0.38 and 0.31 $e/Å^3$) are displaced along z by 0.84(5) and 0.73(10) Å from Cu toward O and N (Fig. 2), respectively. At 300 K, these peaks are less pronounced (0.24 $e/Å^3$). These difference electron density peaks near the Cu and O, N, C positions evidence the delocalization of electron density in the O-Cu-N≡C bonds. No smearing of the electron density near copper atoms or an increase of their anisotropic displacement parameters is observed; the mean-square displacement amplitudes are very small (see Table I). This implies the absence of a static and/or dynamic Jahn–Teller effect at low temperatures.

B. Electronic structure and charge density distribution

Electronic DOS's have been calculated for the crystal structures determined at temperatures 80 and 340 K. Since both structures have almost indistinguishable DOS features, we present here the results for the $T=80$ K structure. In Fig. 3, we show the partial Cu d, Cl p, N p, O p, and C p DOS's in the range of energies between −4 and 4 eV obtained from non-spin-polarized GGA[25] calculations. We observe a very narrow and sharp contribution of Cu d and Cl, N, and O p states at the Fermi level that are well separated from the rest of the valence and conduction states. These features indicate that these states strongly hybridize and that the system is almost zero dimensional, formed by well isolated Cu tetrahedra. The bandwidth at the Fermi level is less than 0.2 eV (see the inset of Fig. 3, wherein a blowup of the DOS at the Fermi level is shown). From the calculations of the crystal field splitting, we conclude that the Cu d band at the Fermi level has a d_{z^2} character (in the local reference frame of the $CuCl_3ON$ trigonal bipyramid).

Within the GGA,[25] we obtain that the Cu d states are partially occupied and, therefore, the system is metallic. This is a well-known drawback of DFT calculations within the local density approximation (LDA) or GGA approach when performed for correlated systems. Improved exchange-correlation functionals, such as LDA+U,[32] should provide the correct insulating behavior of the material. In the case of $Cu_4OCl_6daca_4$, calculations at the level of spin-polarized GGA already open a small gap at the Fermi level, as shown in Fig. 4. In this figure, we present the partial DOS for Cu d states in both spin-up (upper panel) and spin-down (lower panel) channels. The occupation of the spin-up and spin-down Cu d states is very similar; therefore, the resulting localized magnetic d moment is small. Table II presents the magnetic moment at the cluster core inside the muffin-tin radii. The unpaired Cu electron is strongly delocalized via

TABLE II. Magnetic moment (M, in m_B/atom) within the muffin-tin radii (r_{mt}) and its total moment fraction (%). For the interstitial, the moment is normalized per formula unit (f.u. $=CuO_{0.25}Cl_{1.5}daca$).

Atom	r_{mt}	M	
Cu	2.1	0.583 50	58
O	1.4	0.442 04	11
Cl1	1.6	0.083 52	8.3
Cl2	1.6	0.090 27	4.5
N1	1.2	0.028 57	2.9
Interstitial		0.144 77	14

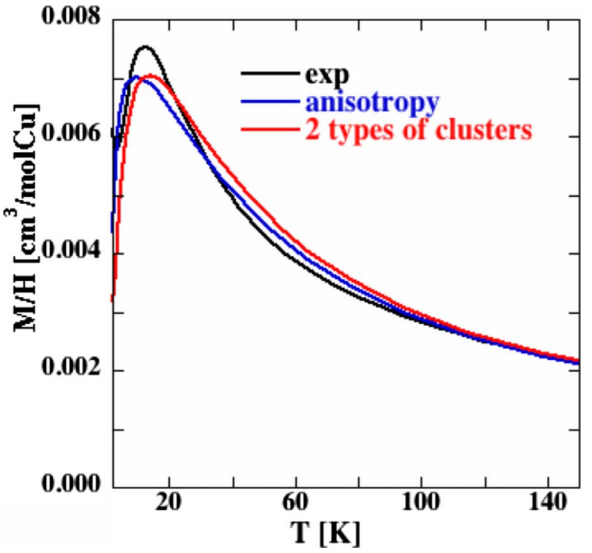

FIG. 8. (Color online) Experimental dc magnetization (M/H) of the single crystal Nr. 1 (black) and the calculated susceptibility for (i) two types of clusters, AF and AF/F, with two AF $J_1=-1.8$ meV, and four F $J_2=1.8$ meV (red); (ii) one type of tetrahedral clusters with $J_{iso}=-1.8$ meV and $J_z=1.2$ meV (blue).

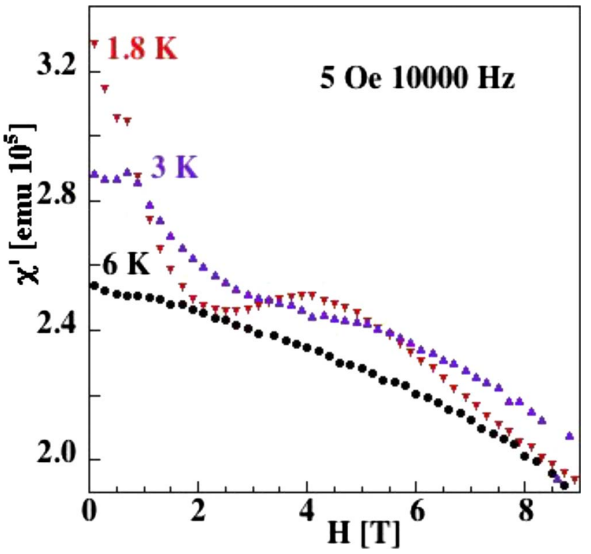

FIG. 9. (Color online) Real part of the ac susceptibility of polycrystalline $Cu_4OCl_6daca_4$ measured in an applied magnetic field of up to 9 T at 1.8, 3, and 6 K.

hybridization mainly with oxygen and less strongly with chlorine and nitrogen.

In Fig. 5, we show the projection on the xy plane of the calculated charge density map of the band around the Fermi level. We note the good agreement with the measured difference Fourier map from the 80 K x-ray diffraction experiment (Fig. 2).

C. Bulk properties

The temperature dependence of dc magnetization (M/H) measured for the polycrystalline sample at $H=0.1$ T and for a single crystal (Nr. 1) at several values of applied magnetic field is presented in Fig. 6. At 300 K, the $(M/H)T$ value is 0.375 cm^3(mol Cu)$^{-1}$ K, suggesting that the system is composed of uncoupled $S=1/2$ spins. The Curie–Weiss temperature estimated from the high-temperature susceptibility is $\theta_1=-50$ K, which implies dominant antiferromagnetic interactions.

For the polycrystalline sample, M/H gradually increases with temperature lowering and at 1.8 K reaches 0.02 cm^3(mol Cu)$^{-1}$. This is a very small value, suggesting the presence of a tiny amount of free $S=1/2$ impurities. However, the temperature dependence cannot be fitted to a Curie-type $1/T$ contribution, which would grow much faster at low temperatures. For a single crystal, dc magnetization consists of two major contributions. The first contribution has a bump near 12 K and can be attributed to isolated tetrahedra with antiferromagnetic exchange with $J=-1.8$ meV resulting in a spin-singlet ground state. The second contribution increases with temperature decrease and, similar to the polycrystalline case, cannot be fitted to the paramagnetic $1/T$ term. The ratio of these contributions is different for different single crystals and depends on the crystal orientation and the applied magnetic field. Based on a number of dc magnetization measurements, we reckon that the ratio of these contributions and the sensitivity to magnetic field is related not to a specific crystallographic direction but to the morphology of crystal. Apparently, there is a strong growth anisotropy and not a lattice anisotropy.

Crystals usually grow as platelets with the [110] axis directed along the shortest edge and [001] and $[\bar{1}10]$ being in the basal plane. An example of M/H utmost sensitivity to the field is presented in the inset of Fig. 6. The measurement is performed with the magnetic field applied along the shortest edge. With increasing field, the bump at low temperatures decreases and already vanishes at $H=0.5$ T.

For another crystal (Nr. 2), M/H shows no bump along the shortest edge even at $H=0.2$ T (Fig. 7), although when the magnetic field is applied along the middle [001] or long $[\bar{1}10]$ edges of the crystal, the bump is tractable to much higher fields (not shown).

One more important observation is that the low-field (0.05 T) dc-magnetization curves measured for the zero-field cooled and 0.05 T cooled conditions are different (not shown). This implies that cooling in a relatively small field is sufficient to change the microscopic state of the crystal.

The field dependence of dc magnetization is also sample and direction dependent (Fig. 7 inset). For the polycrystalline sample, magnetization is concave and does not saturate at 14 T, reaching only $0.27m_B$/Cu. For the Nr. 2 single crystal, magnetization attains almost $0.5m_B$/Cu for the [110] direction, while for other directions it approaches values similar to those for the polycrystalline sample.

The most plausible origin of our observations is the presence of nonuniform intratetrahedral exchange couplings within a single crystal and—even to a larger extent—within a polycrystalline sample. This diversity most probably appears due to the manifold of molecular configurations above the order-disorder crossover at $T_C=282$ K, which could influence the microscopic state of the system in two ways: (i)

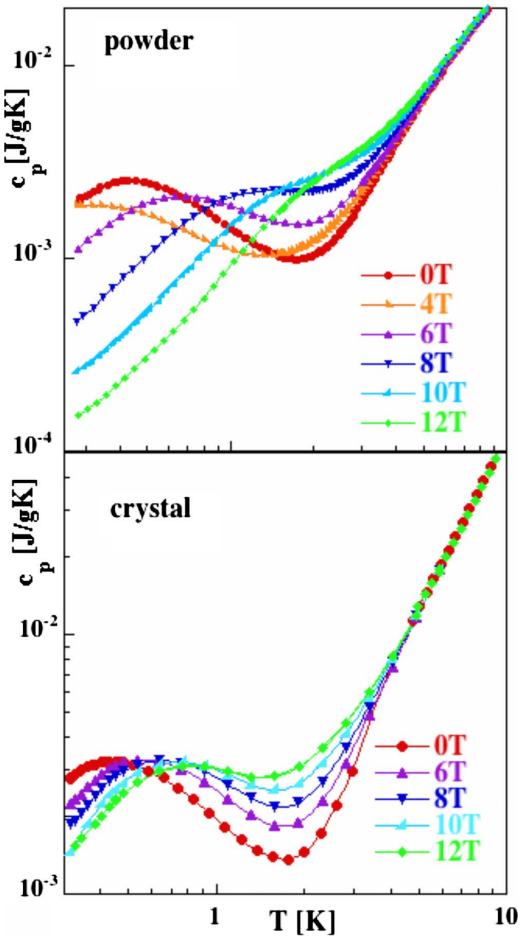

FIG. 10. (Color online) Log-log plots of specific heats of polycrystalline (top) and single crystal (bottom) $Cu_4OCl_6daca_4$ in the 0.28–10 K temperature range with applied magnetic fields of 0–12 T.

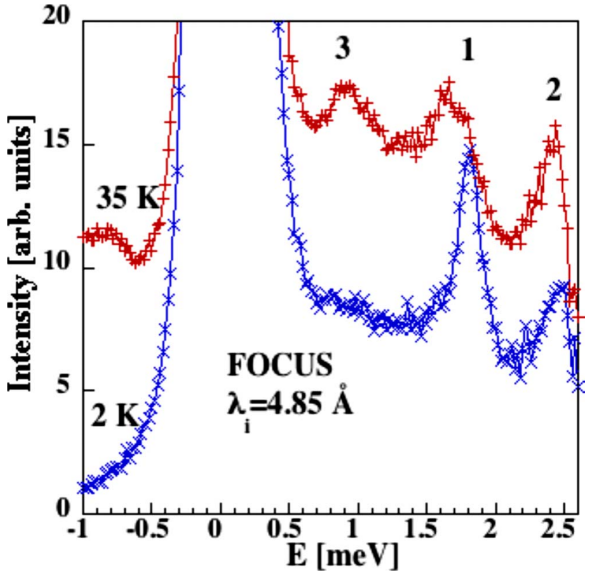

FIG. 11. (Color online) INS spectra of protonated $Cu_4OCl_6daca_4$ at $T=2$ K (blue) and 35 K (red) measured on FOCUS with $\lambda_i = 4.85$ Å. The intensity has been integrated over the momentum transfer range $0.5<Q<2$ Å^{-1}.

during the crystal growth, performed at room temperature, several non-ground-state molecular configurations freeze-in; and (ii) during the field cooling through the crossover region, the applied field favors certain non-ground-state molecular configurations. In these frozen-in molecular configurations, the Cl_1 ions could have positions which strengthen the ferromagnetic exchange path between two or more Cu^{2+} ions. As these molecular configurations are minority and do not represent the ground state, we shall call them "defects" for short.

In agreement with the above considerations, it is reasonable to assume a coexistence of at least two kinds of clusters to explain the measured dc magnetization: (i) AF ones, with AF exchange on the order of $J=-1.8$ meV; and (ii) AF/F ones, with F couplings of similar strength as that of the AF ones. The susceptibility calculated for this case (red curve in Fig. 8) fits relatively well the experiment. We can fit our data also with the model comprising large anisotropy of exchange within the single type of clusters (blue curve in Fig. 8), but an unreasonably large anisotropy parameter $J_z=1.2$ meV is required. We therefore give preference to the hypothesis of the presence of two kinds of clusters.

Within the proposed scenario, it is also easy to understand the strong sensitivity of the bulk properties to the applied magnetic field which is significantly smaller than J. The real part of the ac susceptibility of the polycrystalline sample shows several steps as a function of applied field (Fig. 9). The most pronounced step is between 2–4 T, which corresponds to the Zeeman energy of 0.24–0.48 meV. Also, the low-temperature specific heat of the polycrystalline and single crystal samples contains a broad Schottky-type anomaly centered at 0.4 K (0.034 meV) in zero-field data (Fig. 10). This feature shifts to higher temperatures with an applied field. The magnetic entropy extracted below 10 K after subtraction of a constant phonon contribution reaches only 0.7–0.8 J/K mol Cu. This is approximately 1/8 of the $R \ln 2 = 5.763$ J/K mol Cu value expected for the spin degree of freedom, so this magnetic contribution corresponds to a minor part of the sample. We deduce that one of the triplet E levels of the AF/F clusters is situated at 0.4 K, although the collected data are insufficient to propose the full energy scheme for AF/F clusters.

D. Inelastic neutron scattering

For the protonated sample at 2 K, two sharp features have been detected at 1.8 and 2.4 meV on the neutron energy loss side; they are labeled 1 and 2 in Fig. 11. The peaks are at least two times broader than the resolution function (0.08 meV at 1.8 meV). At higher temperatures (7, 15, and 35 K), the 1.8 meV feature broadens and shifts to lower energies or a second peak at the slightly lower energy of 1.6 meV appears and increases in intensity, while the 1.8 meV peak decreases. The 2.5 meV feature increases in intensity and an additional feature at 1 meV (labeled 3) appears. No extra peaks have been observed in the low-energy region down to 0.4 meV.

A number of peaks are observed at higher energy transfers (not shown), of which the most pronounced is the one at 4.8

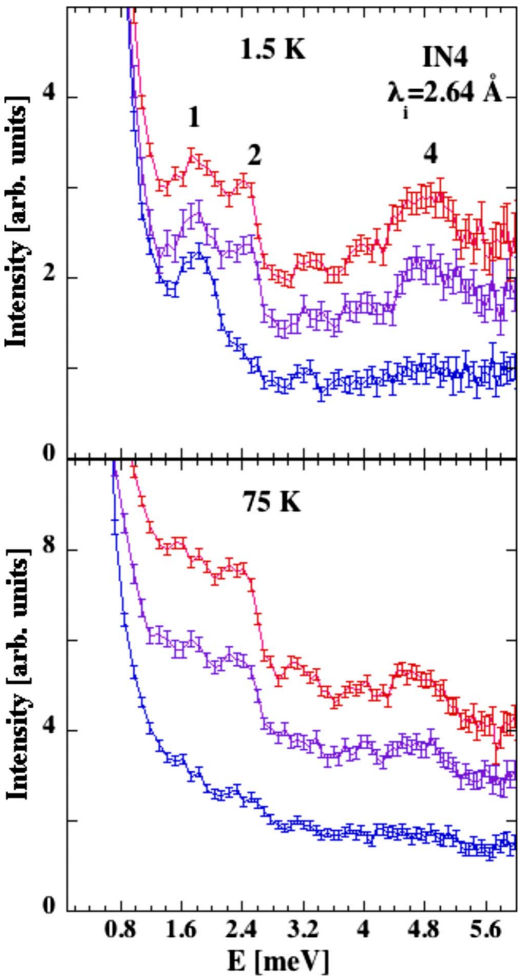

FIG. 12. (Color online) INS spectra of deuterated $Cu_4OCl_6daca_4$ at $T=2$ K (top) and 75 K (bottom) measured on IN4 with $\lambda_i=2.64$ Å for three Q values 1.5 $Å^{-1}$ (blue), 2.5 $Å^{-1}$ (violet), and 3.5 $Å^{-1}$ (red), with increasing intensity integrated over 0.5 $Å^{-1}$.

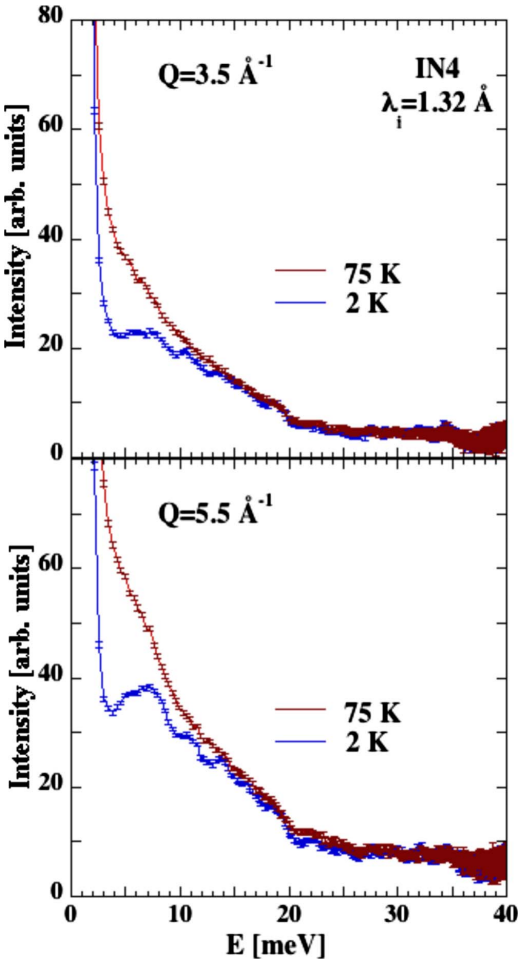

FIG. 13. (Color online) INS spectra of deuterated $Cu_4OCl_6daca_4$ at $T=2$ K and 75 K measured on IN4 with $\lambda_i=1.32$ Å. The intensity has been integrated for two Q values of 3.5 and 5.5 $Å^{-1}$ over 1 $Å^{-1}$.

meV. Its width is at least three times broader than the resolution function (0.3 meV at 4.8 meV), and its intensity increases from 2 to 35 K. The measurements on the deuterated sample reveal essentially the same excitation spectrum (Fig. 12). The 1.8 meV peak tends to vanish at 75 K, while the 2.4 and 4.8 meV features decrease from 2 to 75 K. From the Q (momentum) and T (temperature) dependences, we relate the 1.8 meV peak to a spin singlet-triplet transition between the cluster levels, although it is not clear if it is a single excitation or several ones. It clearly corresponds to the bump in M/H. The 4.8 meV feature increases with Q and most probably is related to molecular vibrations, while for the 2.4 meV and other features the FOCUS and IN4 results are less conclusive.

The measurement at higher energy transfers showed that relatively sharp peaks discussed above reside on a very broad feature (up to 20 meV), which increases in intensity with temperature and Q (Fig. 13). These spectral features and their magnetic or phonon origin are understood with the help of AIMD simulations (discussed below), which reproduce the inelastic scattering response and allow deeper insight via partial vibrational densities of states and specific two-, three-, or four-atom correlation functions.

E. Molecular dynamics

AIMD simulations give a direct view of the amplitude of atomic displacements. While the light atoms tend to have larger displacements than the heavier atoms (Cl and Cu), this is not the case for O which is trapped in the Cu tetrahedron and the Cl octahedron. Note that the atoms are classical particles in the AIMD simulations, so their displacements do not include zero-point motion, which can be on the order of 30% for hydrogen at room temperature. Calculated mean-square displacements averaged over all atoms of the same type are 0.0177 $Å^2$ for Cu, 0.0300 $Å^2$ for Cl, 0.0093 $Å^2$ for O, and 0.0283 $Å^2$ for N. This is in good agreement with values obtained by projection on specified bond directions from the 80 K crystal structure refinement listed in Table I.

The MD simulations are validated by comparing the calculated and measured scattering functions. We note that the low frequency modes are independent of hydrogen or deuterium (H/D) substitution and must therefore be delocalized modes involving many atoms. An acoustic phonon would show a 2% frequency shift upon deuteration. Figure 14 shows the coherent scattering function $S_{coh}(Q,\omega)$ from the 27 ps simulation on the deuterated system. Spectra at lower

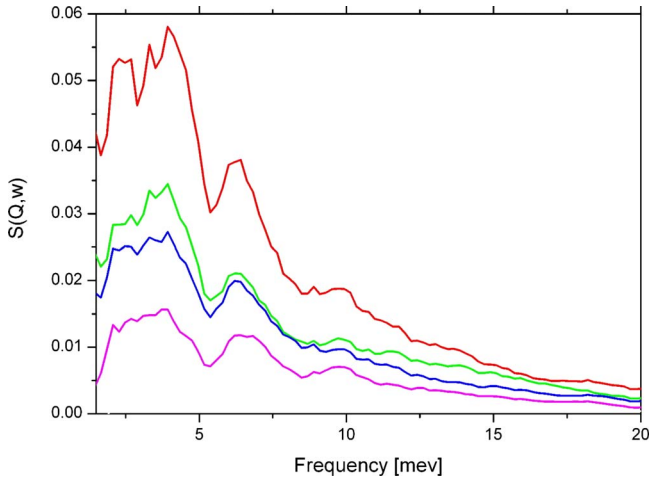

FIG. 14. (Color online) Calculated coherent scattering function for four Q values ranging, with increasing intensity, from 2.5 to 5.5 $Å^{-1}$ of deuterated $Cu_4OCl_6daca_4$.

Q values have weak intensity and are not reliably calculated with our model. Low frequency, numerical noise in the vDOS's contributes strongly to the coherent structure factor since this quantity is proportional to vDOS/frequency. At high Q, there are peaks at 2, 4.5, and 7 meV and a shoulder at $\approx$10 meV, which are consistent with the experimental data (Figs. 11–13). Since the AIMD simulations do not include spin degrees of freedom, these peaks can only be the signature of lattice excitations and, as expected, their intensities increase with increasing Q. The coherent scattering function is calculated only at the reciprocal lattice points of the simulation cell so that Q sampling is limited to the Brillouin zone center when using a single cell for the MD simulations. Simulated spectral peaks therefore correspond to Γ-point modes. Atomic contributions to the signal are obtained from the pvDOS which are shown in the top panel of Fig. 15. Each pvDOS has been normalized to the corresponding number of degrees of freedom, $3n$, where n is the number of a particular species. Fairly well-defined peaks exist at the lowest frequencies in the low-temperature MD simulations. The delocalized nature of the modes is shown by the fact that all atoms have similar pvDOS's below $\approx$5 meV. This result is consistent with there being a negligible spectral shift upon deuteration. The trapped oxygen atom has a characteristic vibration frequency on the order of 55 meV, and this is the only atom that does not contribute to the lowest frequency modes. The analysis of the chlorine atoms has been refined to separate the contributions from apical atoms and those in the square base around the copper tetrahedron. There is a small but significant softening of the apical-chlorine vibrations compared to those of the square-base chlorines, with the average frequencies and standard deviations being, respectively, 18.8 ± 13.5 and 20.3 ± 14.4 meV. The bottom panel of Fig. 15 shows examples of the lowest frequency part of the vDOS's for D, C, and Cu for different lengths of simulations. The dotted curves show the results from a 10 ps trajectory, while the solid curves are derived from the 27 ps trajectory. The longer trajectory gives better frequency resolution, which shows that the first peaks in the DOS occur at

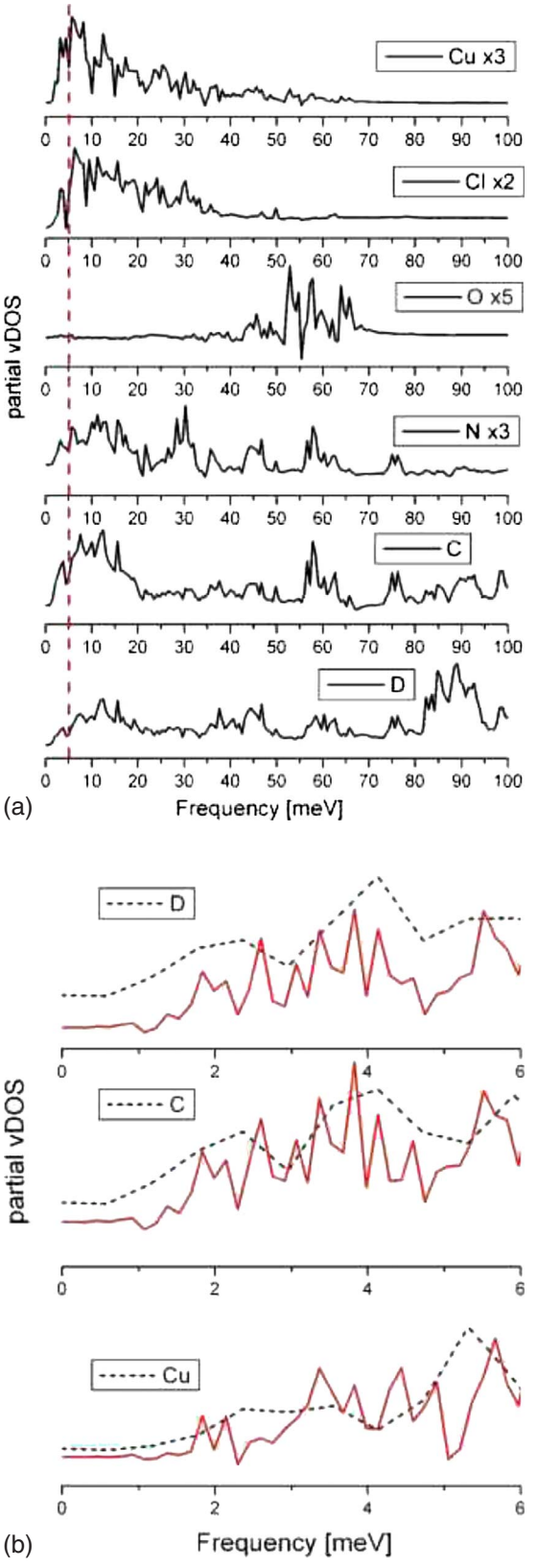

FIG. 15. (Color online) Vibrational density of states for each atom type (top). The vertical dashed line highlights the pronounced minima at 5 meV in all partial DOS's (except for the oxygen vDOS) and the existence of lower frequency modes. Examples of the latter for deuterium, carbon, and copper, are shown separately (bottom).

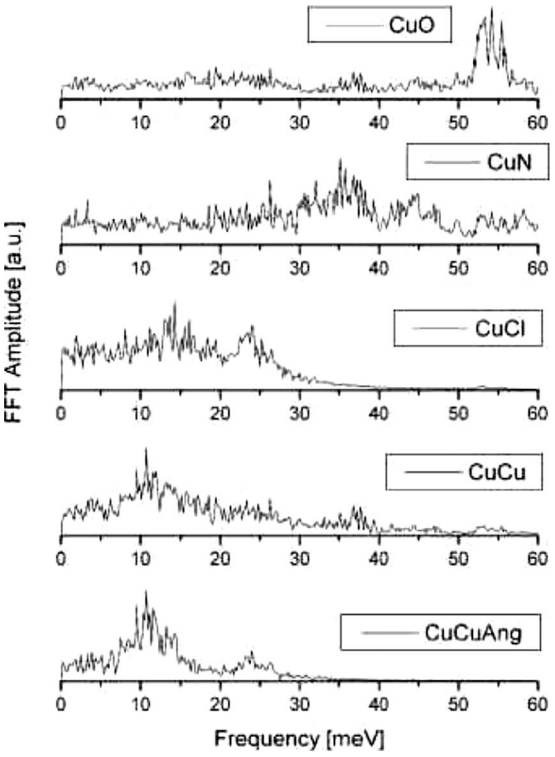

FIG. 16. Two-atom (bond) and four-atom (twist angle) correlations as a function of frequency from the MD calculation.

2 meV. Spectral peaks below this frequency must, therefore, be of magnetic origin.

Features of the VDOS can be further understood by considering *n*-atom correlations. The frequency spectrum of interatomic distances involving Cu atoms is shown in Fig. 16. The Cu-Cu stretch is strongest at ≈ 12 meV. The twisting deformation of the tetrahedron, that is, the angle variation between Cu-Cu vectors on opposite sides of the tetrahedron, also has a characteristic frequency of ≈ 12 meV. These are the modes that could directly modulate the magnetic copper-copper interactions. The oxygen pathway is clearly not modified by any low frequency modes, whereas the copper-chlorine distance modulations show a significant amplitude from 25 meV down to the lowest frequencies.

Spin restricted AIMD simulations are the only way to gain insight into the low frequency modes measured on FOCUS and IN4. The simulations show excitations at above 2 meV and at ≈ 4.5 meV, which grow in intensity with Q and therefore correspond mainly to molecular vibrations. Below these frequencies, the longest simulations (27 ps) indicate that there are no lower lying lattice vibrations, implying that the lower-energy features observed in the experiment are of magnetic origin.

V. SUMMARY

The $Cu_4OCl_6daca_4$ system comprises a very interesting magnetic unit—a Cu^{2+} $S=1/2$ tetrahedron. Due to the geometry of the cluster, two exchange paths are possible: antiferromagnetic Cu-O-Cu via the central oxygen atom and ferromagnetic Cu-Cl-Cu via the peripheral chlorine atoms. In the ideal system, the AF exchange with $J=-1.8$ meV dominates.

Our DFT calculations show that unpaired electron is only partially localized in the Cu *d* states and hybridizes strongly with the oxygen atom in the center of the tetrahedron and is further delocalized around atomic cores within the molecule. Besides the O^{2-} and Cl^- ions, which certainly participate in the Cu-Cu superexchange, the $N \equiv C$ bond might play an important role of the charge reservoir. We plan to confirm this picture by polarized neutron spin density mapping and to study the interplay between electron delocalization and magnetic interactions in more detail.

The presence of strong molecular vibrations has been observed in our INS experiments and spin restricted AIMD simulations. Although all atoms participate in the vibrations, it is the organic ligands and the apical Cl^- ions of the cluster which vibrate most strongly, while the O^{2-} ion remains pinned in the center of the tetrahedron. Therefore, the spin-vibrational Hamiltonian suggested by Jones[16] and Polinger *et al.*[22,23] might be the appropriate model to describe the ideal $Cu_4OCl_6daca_4$ system.

However, the properties of real samples cannot be that easily attributed to this model. Measurements of the bulk properties of single crystals reveal strong anisotropy which dominates also the bulk properties of polycrystalline samples. We infer that only part of the clusters retain the spin singlet ground state, while another part has magnetic ground state, and the ratio between these fractions is sample and thermal history dependent. The anisotropy originates most probably from defects introduced during the sample synthesis as there is only small energy difference between several molecular configurations. The isostructural order-disorder structural crossover at $T_C=282$ K (Ref. 31) complicates the situation even more, as the applied magnetic field and thermal history may affect which molecular configuration freezes-in, determining in this way the magnetic exchange at low temperatures. In this sense, the high-temperature manifold of molecular configurations governs magnetic exchange at low temperature.

It is well possible that molecular vibrations influence the low-temperature magnetic properties as well; we leave this question open for future investigations. We suspect that unusual magnetic susceptibility measured for other representatives of the $Cu_4OCl_6L_4$ system[13,15,17,21] might have similar origin to $Cu_4OCl_6daca_4$. It is important to note that influence of the structural and vibrational degrees of freedoms on magnetic properties of molecular magnets is recognized in a number of other systems, such as, for example, in $\{V_{15}\}$ complex,[33–35] $\{Ni_4Mo_{12}\}$ spin tetrahedron,[36] and $\{Cu_3\}$ spin triangle.[37]

Finally, the complications of the real samples hinder answering the initial question which motivated our research, namely, whether the ground state of an isolated tetrahedron with antiferromagnetic exchange remains degenerate or whether this degeneracy is easily lifted by some small perturbation. Our study reveals that the behavior of such "simple" systems is quite complex and is governed by the high sensitivity of the electronic structure of the system on the precise molecular configuration and this determines the magnetic behavior of the material.

ACKNOWLEDGMENTS

Discussions with P. Tregenna-Piggott, D. Chernyshov, A. F. Albuquerque, and S. Klonishner are gratefully acknowledged. The work was partially performed at SINQ, Paul Scherrer Institute, Villigen, Switzerland. We are grateful for the technical support on Quantum Design magnetometers of the Universities of Bern and Zürich and acknowledge SNBL for the in-house beamtime allocation.

*oksana.zaharko@psi.ch

[1] C. Waldtmann, H.-U. Everts, B. Bernu, C. Lhuillier, P. Sindzingre, P. Lecheminant, and L. Pierre, Eur. Phys. J. B **2**, 501 (1998).
[2] R. Moessner and J. T. Chalker, Phys. Rev. Lett. **80**, 2929 (1998).
[3] B. Canals and C. Lacroix, Phys. Rev. Lett. **80**, 2933 (1998).
[4] G. Misguich, C. Lhuillier, B. Bernu, and C. Waldtmann, Phys. Rev. B **60**, 1064 (1999).
[5] J. B. Fouet, M. Mambrini, P. Sindzingre, and C. Lhuillier, Phys. Rev. B **67**, 054411 (2003).
[6] M. Johnsson, K. W. Törnroos, F. Mila, and P. Millet, Chem. Mater. **12**, 2853 (2000).
[7] P. Lemmens, K.-Y. Choi, E. E. Kaul, Ch. Geibel, K. Becker, W. Brenig, R. Valentí, C. Gros, M. Johnsson, P. Millet, and F. Mila, Phys. Rev. Lett. **87**, 227201 (2001).
[8] W. Brenig and K. W. Becker, Phys. Rev. B **64**, 214413 (2001).
[9] K. Totsuka and H.-J. Mikeska, Phys. Rev. B **66**, 054435 (2002).
[10] R. Valentí, T. Saha-Dasgupta, C. Gros, and H. Rosner, Phys. Rev. B **67**, 245110 (2003).
[11] C. Gros, P. Lemmens, M. Vojta, R. Valentí, K.-Y. Choi, H. Kageyama, Z. Hiroi, N. V. Mushnikov, T. Goto, M. Johnsson, and P. Millet, Phys. Rev. B **67**, 174405 (2003).
[12] O. Zaharko, A. Daoud-Aladine, S. Streule, J. Mesot, P. J. Brown, and H. Berger, Phys. Rev. Lett. **93**, 217206 (2004).
[13] M. Mambrini, J. Trébosc, and F. Mila, Phys. Rev. B **59**, 13806 (1999).
[14] I. Bose and A. Tribedi, Phys. Rev. A **72**, 022314 (2005).
[15] M. E. Lines, A. P. Ginsberg, R. L. Martin, and R. C. Sherwood, J. Chem. Phys. **57**, 1 (1972).
[16] D. H. Jones, J. Chem. Phys. **79**, 3877 (1983).
[17] A. B. Blake, J. Chem. Soc. Dalton Trans. **1**, 2039 (1997).
[18] L. F. Chibotaru, Koord. Khim. **15**, 634 (1989).
[19] E. Buluggiu, J. Chem. Phys. **84**, 1243 (1986).
[20] T. D. Black, R. S. Rubins, D. K. De, R. C. Dickinson, and W. A. Baker, Jr., J. Chem. Phys. **80**, 4620 (1984).
[21] R. C. Dickinson, W. A. Baker, T. D. Black, and R. S. Rubins, J. Chem. Phys. **79**, 2609 (1983).
[22] V. Z. Polinger, L. F. Chibotaru, and I. B. Bersuker, Mol. Phys. **52**, 1271 (1984).
[23] V. Z. Polinger, L. F. Chibotaru, and I. B. Bersuker, Phys. Status Solidi B **129**, 615 (1985).
[24] E. A. Goreshnik and V. V. Olijnyk, Zh. Neorg. Khim. **41**, 206 (1996).
[25] J. P. Perdew, K. Burke, and M. Ernzerhof, Phys. Rev. Lett. **77**, 3865 (1996).
[26] P. Blaha, K. Schwarz, G. K. H. Madsen, D. Kvasnicka, and J. Luitz, *WIEN2k, An Augmented Plane Wave Plus Local Orbitals Program for Calculating Crystal Properties*, edited by K. Schwarz (Technical University, Wien, Austria, 2001).
[27] G. Kresse and J. Furthmuller, Phys. Rev. B **54**, 11169 (1996).
[28] G. Kresse and J. Hafner, Phys. Rev. B **47**, 558 (1993).
[29] K. Parlinski, in *Neutrons and Numerical MethodsN_2M*, AIP Conf. Proc. No. 476, edited by M. R. Johnson, G. G. Kearley, and H. G. Buttner (AIP, New York, 1999), p. 121.
[30] T. Rog, K. Murzyn, K. Hinsen, and G. Kneller, J. Comput. Chem. **24**, 657 (2003).
[31] Y. Filinchuk, D. Chernyshov, and O. Zaharko (unpublished).
[32] V. I. Anisimov, J. Zaanen, and O. K. Andersen, Phys. Rev. B **44**, 943 (1991).
[33] S. Pillet, M. Souhassou, and C. Lecomte, Acta Crystallogr., Sect. A: Found. Crystallogr. **60**, 455 (2004).
[34] M. A. Aebersold, B. Gillon, O. Plantevin, L. Pardi, O. Kahn, P. Bergerat, I. von Seggern, F. Tuczek, L. Öhrström, A. Grand, and E. Leliévre-Berna, J. Am. Chem. Soc. **120**, 5238 (1998).
[35] I. Chiorescu, W. Wernsdorfer, A. Müller, H. Bögge, and B. Barbara, Phys. Rev. Lett. **84**, 3454 (2000).
[36] J. Schnack, M. Brüger, M. Luban, P. Kögerler, E. Morosan, R. Fuchs, R. Modler, H. Nojiri, R. C. Rai, J. Cao, J. L. Musfeldt, and X. Wei, Phys. Rev. B **73**, 094401 (2006).
[37] K.-Y. Choi, N. S. Dalal, A. P. Reyes, P. L. Kuhns, Y. H. Matsuda, H. Nojiri, S. S. Mal, and U. Kortz, Phys. Rev. B **77**, 024406 (2008).